FIGURE LEGENDS

Fig. 1. Typical temporal bone CT images of the enlarged vestibular aqueduct (EVA) subgroups. (A) aperture enlargement. (B) aperture & midpoint enlargement. (C) midpoint enlargement. (D) borderline enlargement. The midpoint and external aperture of the vestibular aqueduct are indicated by white and black arrows, respectively. As shown in the inset of (A), the midpoint diameter (fine dotted line) and aperture diameter (coarse dotted line) were measured perpendicular to the long axis (white solid line) of the vestibular aqueduct.

Fig. 2. Number of subjects with or without *SLC26A4* mutation alleles in each EVA subgroup. Asteriscs; significant difference (P <0.0125)

Fig. 3. The location of each mutation in *SLC26A4*, the evolutionary conservation of the amino acids ,and nucleotides affected by the novel missense and splice site mutations. (A) location of the *SLC26A4* mutations found in this study. Putative transmembrane regions are shown in black. N-term G; sulfate transporter N-terminal domain with Gly motif, Sulf-T; Sulfate transporter family domain, STAS; Sulphate transporter and anti-sigma factor antagonist domain. (B) electropherograms of the novel mutations and the corresponding sequence from normal alleles. Note that the nucleotide sequence of c.1708-32_1708-16del is shown reverse complementary. (C) upper; multiple alignments

of SLC26A4 protein orthologues at two non-contiguous regions. Arrows indicate affected amino acids. Conserved amino acids are shaded in gray. lower; boundaries between the intron15 and exon16 and deleted nucleotides are indicated at the bottom.

Fig. 4. Association of EVA subgroups with *SLC26A4* genotypes or characteristics of hearing loss in subjects with biallelic *SLC26A4* mutations. (A) proportion of *SLC26A4* genotypes in subjects of each EVA subgroup. (B) proportion of different hearing levels in ears of each EVA subgroup. (C) prevalence of fluctuating hearing loss in subjects of each EVA subgroup. (D) prevalence of progressive hearing loss in subjects of each EVA subgroup.

Table I. Criteria for the subgroups of enlarged vestibular aqueduct

Enlarged vestibular aqueduct subgroup	Midpoint diameter	External aperture diameter
Aperture enlargement	≧1.5 mm	Wider than midpoint
Aperture and midpoint enlargement	≧1.5 mm	Equal to midpoint
Midpoint enlargement	≧1.5 mm	Narrower than midpoint
Borderline enlargement	1.0 mm to <1.5mm	1.0 mm to <1.5mm

Table II. Types of SLC26A4 mutations and characteristics of hearing loss in 34 subjects with Pendred syndrome or DFNB4 by EVA subgroups.

			Allele 1			Allele 2						
EVA morhpology	diagnosis age of deafness (y)	age (y)	exon/ intron	DNA change	amino acid change or splicing mutation	exon/ intron	DNA change	amino acid change or splicing mutation	truncating/non -truncating	hearing level R/L** (dBHL)	fluctuation of hearing	progression of hearing loss
Aperture enlargement	0	1	Intron15	c.1707+5G>A	**Splice site mutation**	19	2106-2110dup5	**Q705Wfs18**	**T/T**	90/70#	-	+
	0	33	15	1652insT	**S551Ffs13**	19	c.2168A>G	**p.H723R**	**T/N**	95/95	-	+
	2	6	Intron7	c.919-2A>G	**Splice site mutation**	19	c.2168A>G	**p.H723R**	**T/N**	53.75/63.75	-	+
	0	27	Intron7	c.919-2A>G	**Splice site mutation**	19	c.2168A>G	**p.H723R**	**T/N**	98.75/100	+	+
	0	1	Intron15	c.1707+5G>A	**Splice site mutation**	19	c.2168A>G	**p.H723R**	**T/N**	85##	Unknown	+
	0	31	Intorn5	c.601-1G>A	**Splice site mutation**	19	c.2168A>G	**p.H723R**	**T/N**	73.75/60	+	+
	3	11	Intorn5	c.601-1G>A	**Splice site mutation**	19	c.2168A>G	**p.H723R**	**T/N**	70/87.5	+	+
	0	4	Intron15	c.1707+5G>A	**Splice site mutation**	2	c.82A>G*	**p.S28G***	**T/N**	61.25/61.25	-	Unknown
	0	35	Intorn5	c.601-1G>A	**Splice site mutation**	10	c.1229C>T	**p.T410M**	**T/N**	80/73.75	+	+
	3	12	19	c.2168A>G	**p.H723R**	19	c.2168A>G	**p.H723R**	**N/N**	82.5/106.25	+	+
	3	3	19	c.2168A>G	**p.H723R**	19	c.2168A>G	**p.H723R**	**N/N**	62.5/73.75	-	-
	0	4	19	c.2168A>G	**p.H723R**	19	c.2168A>G	**p.H723R**	**N/N**	55/70	+	-
	0	2	19	c.2168A>G	**p.H723R**	19	c.2168A>G	**p.H723R**	**N/N**	37.5##	Unknown	Unknown
	0	1	19	c.2168A>G	**p.H723R**	19	c.2168A>G	**p.H723R**	**N/N**	102.5/115###	-	-
	0	0.5	10	c.1229C>T	**p.T410M**	19	c.2228T>A	**p.L743X**	**N/N**	73.75##	Unknown	Unknown
	0	1	9	c.1115C>T	**p.A372V**	10	c.1226G>A	**p.R409H**	**N/N**	92.5##	-	-
	0	20	19	c.2168A>G	**p.H723R**	14	c.1579A>C	**p.T527P**	**N/N**	97.5/101.25	-	-
	0	4	15	c.1667A>G	**p.Y556C**	14	c.1579A>C	**p.T527P**	**N/N**	77.5/75	-	+
	0	6	3	c.266C>T	**p.P76S**	14	c.1579A>C	**p.T527P**	**N/N**	17.5/93.75	-	+
	0	9	10	c.1174A.>T	**p.N392Y**	19	c.2162C>T	**p.T721M**	**N/N**	103.75/110	+	+
Aperture & midpoint enlargement	0	15	Intron15	c.1708-32_1708-16del*	**Splice site mutation***	19	c.2168A>G	**p.H723R**	**T/N**	76.25/91.25	+	+
	0	9	Intron7	c.919-2A>G	**Splice site mutation**	17	c.2007C>A*	**p.D669E***	**T/N**	100/100	+	-
	0	1	19	c.2168A>G	**p.H723R**	14	c.1579A>C	**p.T527P**	**N/N**	115##	-	-
	5	6	19	c.2168A>G	**p.H723R**	19	c.2168A>G	**p.H723R**	**N/N**	47.5/62.5	-	-
	1	2	19	c.2168A>G	**p.H723R**	19	c.2168A>G	**p.H723R**	**N/N**	105/93.75###	Unknown	Unknown
Midpoint enlargement	0	3	Intron7	c.919-2A>G	**Splice site mutation**	17	c.2007C>A*	**p.D669E***	**T/N**	82.5/93.75####	+	+
	0	8	19	c.2168A>G	**p.H723R**	18	c.2074T>C*	**p.F692L***	**N/N**	75/115	+	+
	7	10	19	c.2168A>G	**p.H723R**	19	c.2168A>G	**p.H723R**	**N/N**	60/15	+	+
	0	35	10	c.1229C>T	**p.T410M**	17	c.1975G>C	**p.V659L**	**N/N**	97.5/87.5	+	+

Borderline enlargement	0	5	Intron7	c.919-2A>G	**Splice site mutation**	19	c.2168A>G	**p.H723R**	**T/N**	73.75/77.5	+	+
	2	2	intron14	c.1614+1G>A	**Splice site mutation**	10	c.1229C>T	**p.T410M**	**T/N**	55##	Unknown	Unknown
	4	4	19	c.2168A>G	**p.H723R**	19	c.2168A>G	**p.H723R**	**N/N**	106.25/88.75####	Unknown	+
	0	6	14	c.1586T>G	**p.I529S**	19	c.2168A>G	**p.H723R**	**N/N**	80/66.25	-	-
	4	14	10	c.1229C>T	**p.T410M**	19	c.2168A>G	**p.H723R**	**N/N**	118.75/58.75	+	+

*, candidate novel mutation; **, value without slash indicates binaural stimulus; #, ABR; ##, COR; ###, ASSR ; ####, play

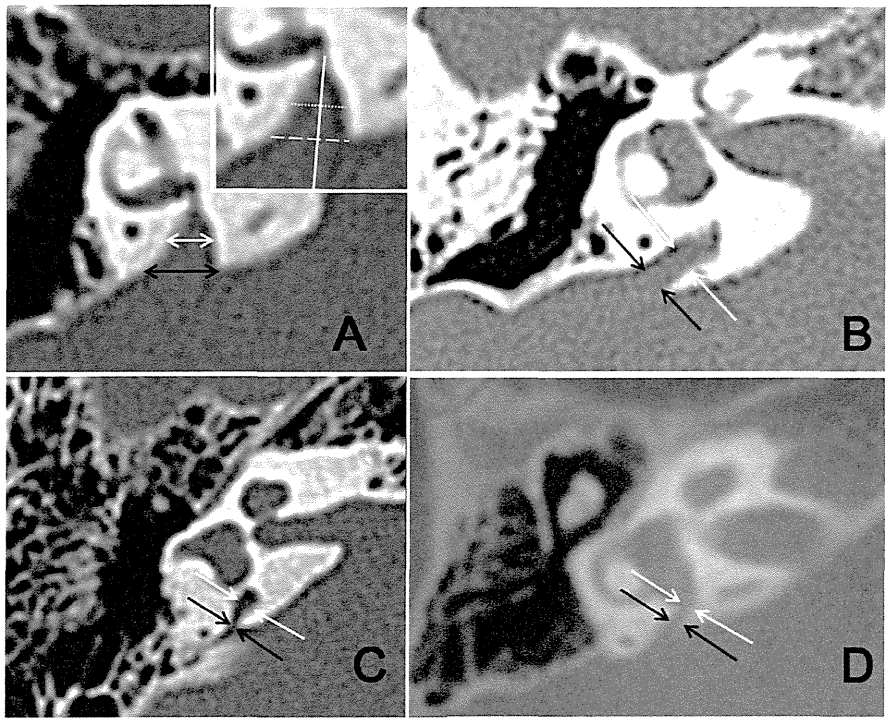

Fig. 1

Typical temporal bone CT images of the enlarged vestibular aqueduct (EVA) subgroups. (A) aperture enlargement. (B) aperture & midpoint enlargement. (C) midpoint enlargement. (D) borderline enlargement. The midpoint and external aperture of the vestibular aqueduct are indicated by white and black arrows, respectively. As shown in the inset of (A), the midpoint diameter (fine dotted line) and aperture diameter (coarse dotted line) were measured perpendicular to the long axis (white solid line) of the vestibular aqueduct.

184x160mm (150 x 150 DPI)

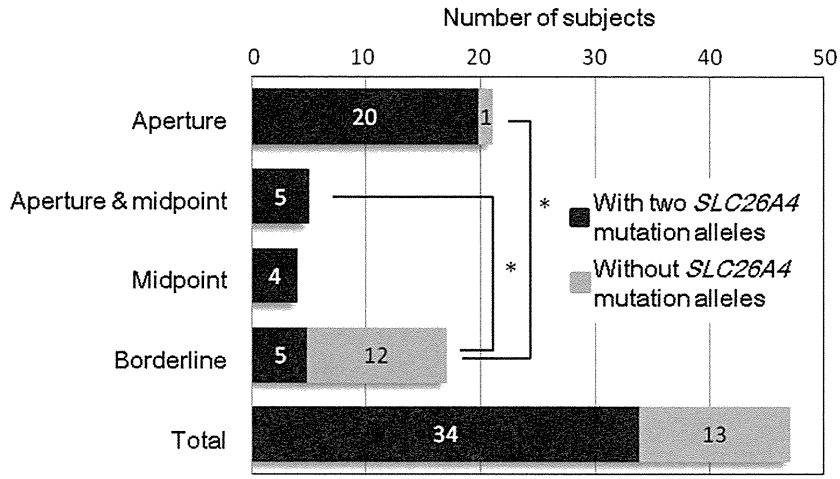

Fig.2

Number of subjects with or without SLC26A4 mutation alleles in each EVA subgroup. Asteriscs; significant difference (P <0.0125)
130x100mm (150 x 150 DPI)

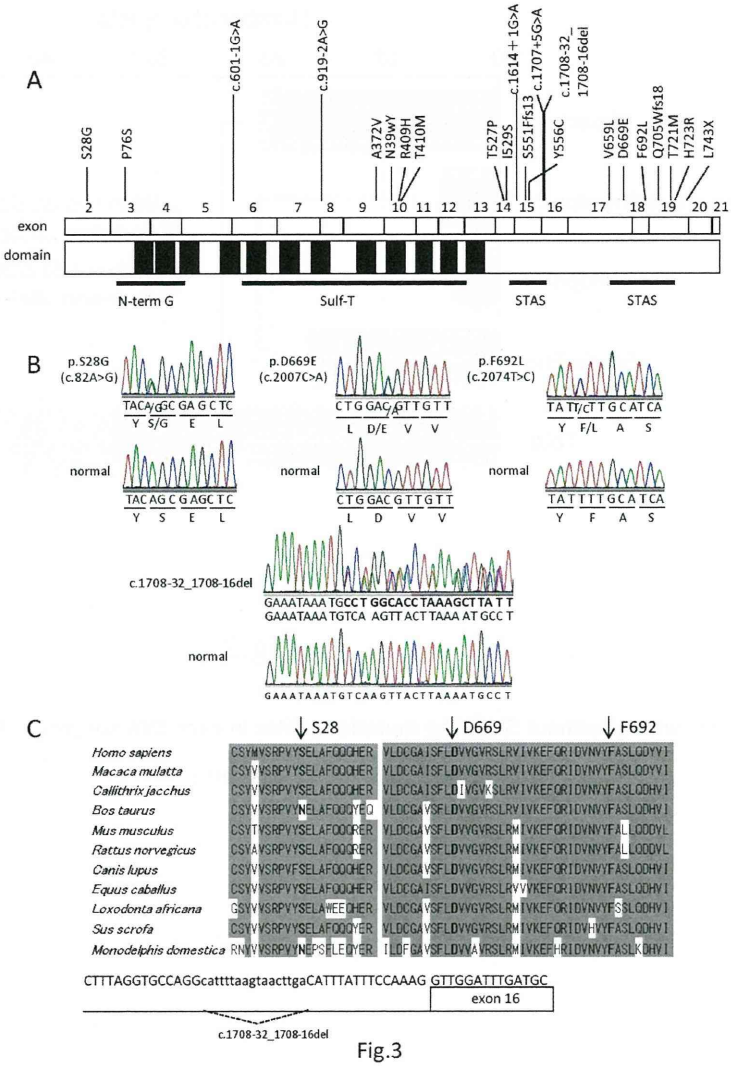

Fig.3

The location of each mutation in SLC26A4, the evolutionary conservation of the amino acids ,and nucleotides affected by the novel missense and splice site mutations. (A) location of the SLC26A4 mutations found in this study. Putative transmembrane regions are shown in black. N-term G; sulfate transporter N-terminal domain with Gly motif, Sulf-T; Sulfate transporter family domain, STAS; Sulphate transporter and anti-sigma factor antagonist domain. (B) electropherograms of the novel mutations and the corresponding sequence from normal alleles. Note that the nucleotide sequence of c.1708-32_1708-16del is shown reverse complementary. (C) upper; multiple alignments of SLC26A4 protein orthologues at two non-contiguous regions. Arrows indicate affected amino acids. Conserved amino acids are shaded in gray. lower; boundaries between the intron15 and exon16 and deleted nucleotides are indicated at the bottom.
176x252mm (150 x 150 DPI)

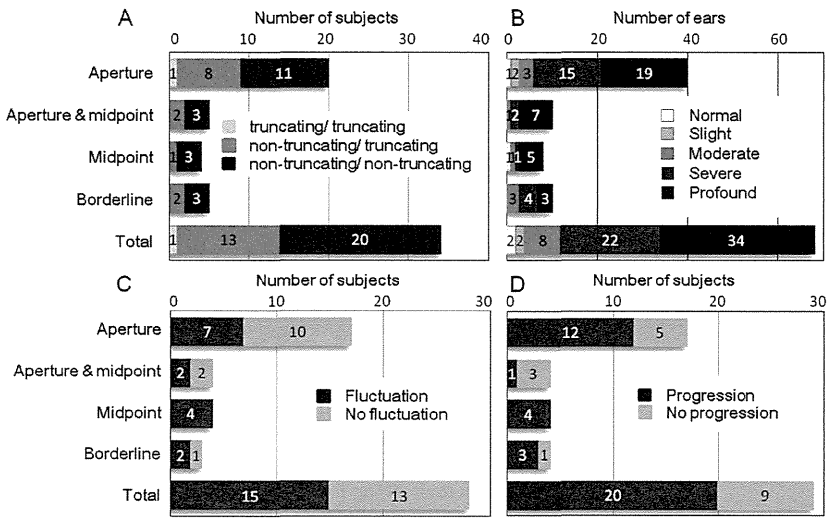

Fig.4

Association of EVA subgroups with SLC26A4 genotypes or characteristics of hearing loss in subjects with biallelic SLC26A4 mutations. (A) proportion of SLC26A4 genotypes in subjects of each EVA subgroup. (B) proportion of different hearing levels in ears of each EVA subgroup. (C) prevalence of fluctuating hearing loss in subjects of each EVA subgroup. (D) prevalence of progressive hearing loss in subjects of each EVA subgroup.
193x141mm (150 x 150 DPI)

G Model
NSR-3579; No. of Pages 9

ARTICLE IN PRESS

Neuroscience Research xxx (2013) xxx–xxx

Contents lists available at SciVerse ScienceDirect

Neuroscience Research

journal homepage: www.elsevier.com/locate/neures

Long-lasting changes in the cochlear K^+ recycling structures after acute energy failure

Yoichiro Takiguchi[a,b,c], Guang-wei Sun[b,1], Kaoru Ogawa[c], Tatsuo Matsunaga[b,*]

[a] Department of Otolaryngology, Eiju General Hospital, 2-23-16 Higashi-ueno, Taito-ku, Tokyo 110-8645, Japan
[b] The Laboratory of Auditory Disorders, National Institute of Sensory Organs, National Tokyo Medical Center, 2-5-1 Higashigaoka, Meguro-ku, Tokyo, 152-8902, Japan
[c] Department of Otolaryngology, School of Medicine, Keio University, 35 Shinanomachi, Shinjuku-ku, Tokyo, 160-8582, Japan

ARTICLE INFO

Article history:
Received 2 February 2013
Received in revised form 30 April 2013
Accepted 8 June 2013
Available online xxx

Keywords:
Hearing loss
Mitochondrial dysfunction
3-Nitropropionic acid
Cochlear fibrocytes
Stria vascularis
Recovery

ABSTRACT

Fibrocytes in the cochlear lateral wall and spiral limbus play an important role in transporting K^+ and have the capacity of self-renewal. We showed that acute energy failure in the rat cochlea induced by local administration of the mitochondrial toxin 3-nitropropionic acid (3NP) caused hearing loss in a concentration-dependent manner, mainly due to degeneration of cochlear fibrocytes. We produced long-lasting profound cochlear damage in this model by modifying the 3NP administration protocol and observed morphological changes at 16 weeks after the administration. In the spiral ligament, severe degeneration of fibrocytes was observed in the basal turn, and the levels of the Na,K-ATPase alpha and beta1 subunits and of NKCC1 were decreased in these cells, whereas connexin 26 (Cx26) level increased in the type 1 fibrocytes adjacent to the stria vascularis. In the stria vascularis, levels of Kir4.1 and L-PGDS decreased. In the spiral limbus, severe degeneration of fibrocytes was observed in the middle and basal turns, but NKCC1 and Cx26 were still found in the center of the limbus in the middle turn. These results indicate long-lasting changes in the cochlear lateral wall and spiral limbus, which may compensate for damaged K^+ recycling and protect cells from ATP shortage.

1. Introduction

Sudden sensorineural hearing loss (SSNHL) is a common cause of otologic emergencies encountered by otorhinolaryngologists, and it has a reported recovery rate of 30–60% (Conlin and Parnes, 2007). SSNHL becomes fixed after 8–12 weeks from onset (Ito et al., 2002), and there is no effective therapy for SSNHL after that period (Slattery et al., 2005). The majority of patients with persistent SSNHL have a perceived handicap associated with tinnitus and hearing loss (Chiossoine-Kerdel et al., 2000). The prevailing theories for the cause of SSNHL are ischemia or viral infection of the cochlea. The cells of the inner ear are considered to be highly susceptible to mitochondrial dysfunction (Fischel-Ghodsian et al., 2004; Pickles, 2004; Hsu et al., 2005), which likely underlies the susceptibility of the inner ear to acute energy failure such as cochlear ischemia (Seidman et al., 1999).

The cochlear lateral wall plays important roles in the physiology of hearing, including the transport of K^+ to generate an endocochlear potential in the endolymph that is essential for transduction of sound by hair cells (Wangemann, 2002). The spiral ligament in the lateral wall consists of five types of fibrocytes based on their structural features, immunostaining patterns, and general location. The stria vascularis consists of three types of cells, including basal cells, intermediate cells, and marginal cells (Spicer and Schulte, 1996) (Fig. 1). It has been suggested that the recycling of K^+ back into the stria vascularis is critical for these functions. It has also been postulated that the cochlear ion transport system, which is essential for hearing, consists of extracellular flow through the scala tympani and scala vestibuli, and transcellular flow through the organ of Corti, supporting cells, and cells of the lateral wall. According to this theory, type 2 and type 4 fibrocytes resorb K^+ from the surrounding perilymph and from outer sulcus cells via Na,K-ATPase and NKCC1 (Na-K-Cl cotransporter isoform 1). The K^+ are then transported to type 1 fibrocytes, stria basal cells, and intermediate cells through gap junctions and then secreted into the intrastrial space through the Kir4.1 channel (an inwardly rectifying K^+ channel). The secreted K^+ are incorporated into marginal cells by Na,K-ATPase and NKCC1 and are finally secreted into the

Abbreviations: SSNHL, sudden sensorineural hearing loss; 3NP, 3-nitropropionic acid; NKCC1, Na-K-Cl cotransporter isoform 1; Cx26, connexin 26; Kir4.1, an inwardly rectifying K^+ channel; L-PGDS, lipocalin-type prostaglandin D synthase; ABR, auditory brainstem response; PBS, phosphate buffered saline.

* Corresponding author. Tel.: +81 3 3411 0111; fax: +81 3 3412 9811.
E-mail address: matsunagatatsuo@kankakuki.go.jp (T. Matsunaga).
[1] The Laboratory of Biomedical Material Engineering, Dalian Institute of Chemical Physics, The Chinese Academy of Sciences, Dalian, China.

0168-0102/$ – see front matter © 2013 Elsevier Ireland Ltd and the Japan Neuroscience Society. All rights reserved.
http://dx.doi.org/10.1016/j.neures.2013.06.003